J. Fluid Mech. (1996), *vol.* 319, *pp.* 171–196

Semi-analytical solution for second-order wave diffraction by a truncated circular cylinder in monochromatic waves

By J. B. HUANG AND R. EATOCK TAYLOR
Department of Engineering Science, University of Oxford, OX1 3PJ, UK

(Received 23 July 1995 and in revised form 28 February 1996)

A complete semi-analytical solution is given for second-order diffraction of monochromatic waves by a truncated vertical circular cylinder in water of uniform finite depth. The methodology presented in detail elsewhere (Eatock Taylor & Huang 1996) is adopted to find a particular solution which exactly satisfies the governing equation, the inhomogeneous free-surface condition and the seabed condition. In order to satisfy the boundary condition on the cylinder bottom, the fluid domain around the cylinder is divided into two regions. First- and second-order velocity potentials are described separately in the two regions and matched on the interface by the pressure and normal-velocity continuity conditions. Based on the formulation, the second-order wave field in the vicinity of the cylinder and the corresponding wave forces and overturning moments on the cylinder are studied in detail. Numerical results for the double frequency forces obtained by using the present semi-analytical approach are compared with those computed with a higher-order boundary element method (Eatock Taylor & Chau 1992). As well as the exact solution, an approximate solution is also given for the second-order potential and the corresponding forces. Numerical results show that the approximate solution possesses excellent accuracy for the total second-order heave force over a wide range of conditions. When $kb > 1.2$ (where k, b are the incident wavenumber and the draught of the cylinder respectively), the accuracy for total second-order surge force and pitch moment is also satisfactory. These results could lead to the development of very efficient solutions and corresponding algorithms for the analysis of second-order wave diffraction by more complicated structures such as tension leg platforms. Numerical results based on the present solution show that in many cases, both the first- and the second-order-free surface elevation in the vicinity of a truncated cylinder is very close to that of a bottom-seated cylinder. For waves with larger amplitudes, the maximum free-surface elevation around a vertical cylinder predicted with the second-order theory can significantly exceed that given by linear theory. There is also a considerable difference in the location of the maximum elevation predicted by the linear and nonlinear theories.

1. Introduction

There has been, in recent years, a considerable number of investigations into nonlinear interactions between water waves and ocean structures, based on potential flow theory. Theoretical approaches to the problem have been mainly based on a perturbation procedure, combined with the boundary-element method. Up to second-order of accuracy, significant progress has been made in this context (see, for example,

Chau 1989; Kim & Yue 1989, 1990; Eatock Taylor & Chau 1992; Chen & Molin 1991; Lee *et al.* 1991). The biggest advantage of the boundary-element method (BEM) is that it can handle wave diffraction by three-dimensional structures of complicated geometry. There are, however, still some problems associated with a boundary element method (BEM) approach: the accuracy of numerical results has a strong dependence on the mesh density and the element shape. Furthermore, for complex geometries, converged second-order results are not easy to obtain and programs based on a BEM implementation at second order are usually very time-consuming to run. Since the coefficient matrix associated with the boundary element method sometimes may be ill-conditioned, special techniques are needed in order to avoid the 'irregular frequency' problem (e.g. Lee & Sclavounos 1989). In view of these problems, analytical or semi-analytical solutions can be very useful in providing 'bench marks' to test the numerical methods. Indeed, for some simpler cases such as cylindrical structures or structures in which cylinders play the major part in diffracting waves, semi-analytical solutions could in principle be used instead of fully numerical methods (for example, by adopting an interaction theory). This may offer a powerful tool for designers, since analytical (or semi-analytical) solutions normally take only a fraction of the CPU time and computer memory as compared with a fully numerical method. This has proved to be very successful for first-order diffraction problems (e.g. McIver & Evans 1984; Kagemoto & Yue 1986; Linton & Evans 1990). Nevertheless, to the authors' knowledge, apart from the simple case of a bottom-seated vertical cylinder extending through the whole water depth (e.g. Kriebel 1990, 1992; Chau & Eatock Taylor 1992), complete semi-analytical solutions to the second-order velocity potential do not appear to exist. Instead, use has been made of the indirect method proposed by Lighthill (1979) and Molin (1979) to estimate second-order wave loads on a single or multiple cylinders. Eatock Taylor & Hung (1987), for example, presented a semi-analytical solution to the second-order wave loads on a bottom-seated vertical circular cylinder; while Williams and his co-authors made a systematic study of the second-order wave loading on both single and arrays of vertical cylinders. Comprehensive results in terms of the total forces on the structures have been obtained (Abul-Azm & Williams 1988, 1989*a*,*b*; Williams, Abul-Azm & Ghalayini 1990; Ghalayini & Williams 1991; Moubayed & Williams 1994, 1995). With the indirect method, however, one cannot obtain the second-order free-surface elevation and the wave run-up on the waterline, which are also important quantities in the design of a floating production system such as a tension leg platform. Another slight disadvantage of the indirect method is that in order to obtain the wave loads associated with different degrees of freedom (e.g. surge, heave, pitch and sway), one has to use different auxiliary radiation potentials. An alternative approach, for the approximate calculation of second-harmonic vertical forces, is based on the asymptotic analysis developed by Newman (1990) for large depths. This has been implemented by Kim (1993) as a tool for preliminary design of deep-draught multi-column structures.

Recently, in connection with the direct solution of the boundary-value problem for the second-order potential, Eatock Taylor & Huang (1996) developed a method for obtaining a particular solution for an axisymmetric structure in regular waves. The resulting solution has been shown to satisfy exactly the inhomogeneous free-surface condition at second order. In this paper, we make use of this methodology to find a particular solution for second-order diffraction by a truncated vertical circular cylinder. Since the particular solution has exactly satisfied the inhomogeneous free-surface condition, the eigenfunction expansion method can then be utilized to find the component of the second-order diffraction potential which satisfies a homogeneous

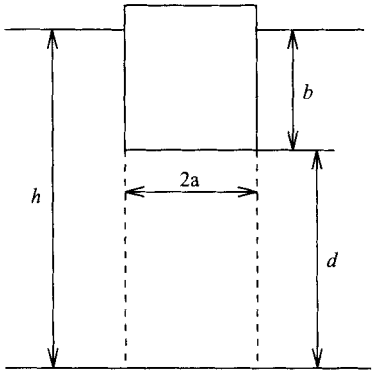

FIGURE 1. Physical diagram and coordinate system for wave-diffraction analysis of a truncated circular cylinder in a monochromatic sea.

free-surface condition. A combination of these two components allows all of the boundary conditions to be satisfied. The solution is analytical in the vertical and circumferential directions, based on appropriate eigen-function and Fourier series expansions. There remains a free-surface integral which is now one-dimensional. In the near field, this integral is evaluated numerically, while in the far field an explicit analytical expression can be obtained (Kim & Yue 1989; Chau & Eatock Taylor 1992). Numerical results are given for the second-order wave loading and the free-surface elevation around truncated cylinders. Effects of different factors are investigated in some detail, and comparisons made with results for bottom-seated cylinders in the same water depth.

2. Formulation of the velocity potential

2.1. *Definition of the boundary-value problem*

We consider the diffraction of a monochromatic incident wave, of frequency ω, wavenumber k and linear amplitude A, by a truncated vertical circular cylinder of radius a and draught b, fixed in water of depth h (see figure 1). Assuming an irrotational flow, we define the velocity potential of the wave field, $\Phi(r,\theta,z,t)$ in a cylindrical polar coordinate system, such that the z-axis coincides with the cylinder axis, originating from the quiescent free surface and pointing upwards. Using the conventional Stokes perturbation procedure, we express $\Phi(r,\theta,z,t)$ as

$$\Phi(r,\theta,z,t) = \mathrm{Re}\{\phi^{(1)}(r,\theta,z)\mathrm{e}^{-\mathrm{i}\omega t} + \phi^{(2)}(r,\theta,z)\mathrm{e}^{-2\mathrm{i}\omega t}\} + \overline{\phi}^{(2)}(x,y,z) + O(\epsilon^3) \qquad (2.1)$$

where $\epsilon = kA$. The steady part of the second-order potential, $\overline{\phi}^{(2)}$, is subsequently neglected, since its contribution to the wave force and the free-surface elevation is at most $O(\epsilon^3)$.

We then divide the fluid domain into two regions: an exterior region (region 1) defined by $a \leqslant r \leqslant \infty$, $0 \leqslant \theta \leqslant 2\pi$, $-h \leqslant z \leqslant 0$, and an interior region (region 2) defined by $0 \leqslant r \leqslant a$, $0 \leqslant \theta \leqslant 2\pi$, $-h \leqslant z \leqslant -b$. The potentials $\phi_j^{(p)}$ ($p = 1,2$; $j = 1,2$; the superscript denoting the order of perturbation and the subscript denoting the number of the flow region) satisfy the following Laplace equation and corresponding boundary conditions:

$$\nabla^2\phi_j^{(p)}(r,\theta,z) = 0 \quad \text{in the fluid domain,} \qquad (2.2)$$

$$\frac{\partial \phi_j^{(p)}}{\partial z} = 0, \quad z = -h, \quad p = 1,2; \quad j = 1,2, \tag{2.3}$$

$$\frac{\partial \phi_2^{(p)}}{\partial z} = 0, \quad z = -b, \quad p = 1,2, \tag{2.4}$$

$$\lim_{r\to\infty} r^{1/2}\left(\frac{\partial \phi_1^{(1)}}{\partial r} - ik\phi_1^{(1)}\right) = 0, \tag{2.5}$$

$$\frac{\partial \phi_1^{(1)}}{\partial z} - v\phi_1^{(1)} = 0, \quad z = 0, \tag{2.6}$$

$$\frac{\partial \phi_1^{(2)}}{\partial z} - 4v\phi_1^{(2)} = q(r,\theta), \quad z = 0, \tag{2.7}$$

where $v = \omega^2/g$, g is the gravitational acceleration, and the wavenumber k satisfies the dispersion equation $k\tanh(kh) = v$. q is the second-order forcing function determined by the first-order potential: its form is given below.

We use the pressure and normal-velocity continuity conditions to match the exterior and the interior regions. This leads to

$$\frac{\partial \phi_1^{(p)}}{\partial r} = \begin{cases} 0, & r = a, \quad -b \leqslant z \leqslant 0 \\ \partial \phi_2^{(p)}/\partial r, & r = a, \quad -h \leqslant z \leqslant -b, \end{cases} \tag{2.8}$$

$$\phi_1^{(p)}(a,\theta,z) = \phi_2^{(p)}(a,\theta,z), \quad -h \leqslant z \leqslant -b, \tag{2.9}$$

where $p = 1,2$. Equations (2.2) to (2.9), plus an appropriate radiation condition for $\phi_1^{(2)}$ (which will be discussed in §2.3), define a complete boundary-value problem for the velocity potentials $\phi^{(1)}$, $\phi^{(2)}$.

2.2. *First-order potential* $\phi^{(1)}$

An accurate and fast evaluation of the first-order diffracted potential is essential for obtaining the second-order diffracted potential. In the case of a truncated vertical circular cylinder, the analytical solution can be obtained using the eigenfunction expansion method. The procedure was described by Garrett (1971) in his analysis of the first-order wave forces on a circular dock, and therefore we will only briefly address it here.

Appropriate expressions for the first-order velocity potentials in the exterior and interior regions are as follows. In the exterior region the potential $\phi^{(1)}$ can be expressed as the sum of the first-order incident potential $\phi_i^{(1)}$ and the first-order diffracted potential $\phi_{d1}^{(1)}$. The former can be written

$$\phi_i^{(1)} = -\frac{igA}{\omega}\frac{\cosh(k(z+h))}{\cosh(kh)}\sum_{n=0}^{\infty} \epsilon_n i^n J_n(kr)\cos(n\theta), \tag{2.10}$$

where $\epsilon_0 = 1, \epsilon_n = 2$ for $n > 0$. The latter can be decomposed into one part $\phi_{d1,1}^{(1)}$ corresponding to diffraction of the incident wave by a bottom-seated vertical cylinder; and a second part $\phi_{d1,2}^{(1)}$ required to enforce the appropriate conditions at $r = a$. Thus

$$\phi_1^{(1)}(r,\theta,z) = \phi_i^{(1)} + \phi_{d1,1}^{(1)} + \phi_{d1,2}^{(1)}, \tag{2.11}$$

leading to

$$\phi_1^{(1)} = \sum_{n=0}^{\infty} \left[\frac{\cosh(k(z+h))}{\cosh(kh)} P_n(kr) + \sum_{j=0}^{\infty} \epsilon_n B_{jn}^{(1)} \frac{U_n(m_j r)}{U_n'(m_j a)} Z_j(m_j, z) \right] \cos(n\theta) \tag{2.12}$$

where

$$P_n(kr) = -\frac{gA}{\omega} \epsilon_n \mathrm{i}^{(n+1)} \left[J_n(kr) - \frac{J_n'(ka) H_n(kr)}{H_n'(ka)} \right], \tag{2.13}$$

$$U_n(m_j r) = \begin{cases} H_n(m_0 r), & j = 0, \\ K_n(m_j r), & j > 0, \end{cases} \tag{2.14}$$

$$Z_0(m_0, z) = \frac{1}{[\gamma_0(m_0)]^{1/2}} \cosh(m_0(z+h)), \quad \gamma_0(m_0) = \frac{h}{2} \left(1 + \frac{\sinh(2m_0 h)}{2m_0 h} \right), \tag{2.15}$$

$$Z_j(m_j, z) = \frac{1}{[\gamma_j(m_j)]^{1/2}} \cos(m_j(z+h)), \quad \gamma_j(m_j) = \frac{h}{2} \left(1 + \frac{\sin(2m_j h)}{2m_j h} \right), \quad j > 0. \tag{2.16}$$

Here $H_n(x)$ is the nth Hankel function of the first kind.

Furthermore, $m_0 = k$ is the wavenumber of the incident wave, and m_j, $j = 1, 2, 3, \cdots$, are the real roots of the dispersion equation:

$$m_j \tan(m_j h) = -v. \tag{2.17}$$

The term $P_n(kr)$ incorporates the contributions from $\phi_i^{(1)}$ and $\phi_{d1,1}^{(1)}$, while the second summation in (2.12) represents $\phi_{d1,2}^{(1)}$.

In the interior region,

$$\phi_2^{(1)} = \sum_{n=0}^{\infty} [\sum_{j=0}^{\infty} \epsilon_n A_{jn}^{(1)} V_n(\lambda_j r) \cos(\lambda_j(z+h))] \cos(n\theta), \tag{2.18}$$

where

$$V_n(\lambda_j r) = \begin{cases} 0.5(r/a)^n, & j = 0, \\ I_n(\lambda_j r)/I_n(\lambda_j a), & j > 0, \end{cases} \tag{2.19}$$

$$\lambda_j = j\pi/(h-b). \tag{2.20}$$

One of the ways of obtaining the linear systems which determine $B_{jn}^{(1)}$ and $A_{jn}^{(1)}$ is to use the eigenfunction expansion approach in $(-h < z < 0)$. Substituting (2.12) and (2.18) into (2.8) and (2.9), we have

$$\{B_n^{(1)}\} = [C_n^{(1)}]\{A_n^{(1)}\}, \tag{2.21}$$

$$\{A_n^{(1)}\} = [D_n^{(1)}]\{B_n^{(1)}\} + \{E_n^{(1)}\}, \tag{2.22}$$

where

$$\{B_n^{(1)}\} = (B_{jn}^{(1)}), \quad \{A_n^{(1)}\} = (A_{jn}^{(1)}), \quad \{E_n^{(1)}\} = (E_{jn}^{(1)}) \quad j = 0, 1, 2, \cdots, \quad n = 0, 1, 2, \cdots, \tag{2.23}$$

$$C_n^{(1)}(j, l) = \frac{V_n'(\lambda_l a)}{m_j h} \int_{-h}^{-b} \cos(\lambda_l(z+h)) Z_j(m_j, z) \mathrm{d}z \quad (l = 0, 1, \cdots, \lambda_0 = 0), \tag{2.24}$$

$$D_n^{(1)}(m, l) = \frac{2}{d} \frac{U_n(m_j a)}{U_n'(m_j a)} \int_{-h}^{-b} \cos(\lambda_l(z+h)) Z_j(m_j, z) \mathrm{d}z \quad (l = 0, 1, \cdots, \lambda_0 = 0), \tag{2.25}$$

$$E_n^{(1)}(l) = \frac{2}{d} P_n(ka) \int_{-h}^{-b} \cos(\lambda_l(z+h)) \frac{\cosh(k(z+h))}{\cosh(kh)} \mathrm{d}z \quad (l = 0, 1, \cdots, \lambda_0 = 0). \tag{2.26}$$

In the above equations, $\{B_n^{(1)}\}$ and $\{A_n^{(1)}\}$ are column vectors of the unknowns, and $\{E_n^{(1)}\}$ is a known column vector. $[C_n^{(1)}]$, $[D_n^{(1)}]$ are matrices of known coefficients, with the subscript n denoting the nth Fourier mode. Expressions for the matrices $C_n^{(1)}$, $D_n^{(1)}$ and the vector $E_n^{(1)}$ are given in Appendix A. It is implied throughout that the infinite series have been truncated appropriately, the issue of convergence being addressed in the section on results.

2.3. *Decomposition of the second-order potential in the exterior region*

In the exterior region, the second-order potential $\phi_1^{(2)}$ can be expressed as the sum of second-order incident potential $\phi_i^{(2)}$ and second-order diffracted potential $\phi_{d1}^{(2)}$

$$\phi_1^{(2)}(r, \theta, z) = \phi_i^{(2)}(r, \theta, z) + \phi_{d1}^{(2)}(r, \theta, z) \tag{2.27}$$

where

$$\phi_i^{(2)} = -\frac{3\mathrm{i}A^2\omega}{8} \frac{\cosh(2k(z+h))}{\sinh^4(kh)} \sum_{n=0}^{\infty} \epsilon_n i^n J_n(2kr) \cos(n\theta). \tag{2.28}$$

We decompose $\phi_{d1}^{(2)}$ into three parts. These correspond to a 'free wave' component due to diffraction of the second-order incident wave by a bottom-seated cylinder, a 'free-wave' component required to enforce the appropriate conditions at $r = a$, and a 'locked wave' due to the first-order forcing on the free surface. Thus

$$\phi_{d1}^{(2)}(r, \theta, z) = \phi_{d1,1}^{(2)} + \phi_{d1,2}^{(2)} + \phi_{d1,3}^{(2)}. \tag{2.29}$$

$\phi_{d1,1}^{(2)}$ and $\phi_{d1,2}^{(2)}$ satisfy the following homogeneous condition on the free surface:

$$\frac{\partial \phi_{d1,j}^{(2)}}{\partial z} - 4\nu \phi_{d1,j}^{(2)} = 0, \quad z = 0, \quad j = 1, 2. \tag{2.30}$$

$\phi_{d1,3}^{(2)}$ satisfies the inhomogeneous free-surface condition obtained from (2.7), where

$$\begin{aligned} q(r, \theta) = \Bigg\{ & -\frac{\mathrm{i}\omega}{2g}(\phi_i^{(1)} + \phi_{d1}^{(1)}) \frac{\partial^2 \phi_{d1}^{(1)}}{\partial z^2} + \frac{\mathrm{i}\omega}{2g} k^2 [6 \tanh^2(kh) - 1] \phi_{d1}^{(1)} \phi_i^{(1)} \\ & + \frac{3\mathrm{i}\omega^5}{2g^3} (\phi_{d1}^{(1)})^2 + \frac{\mathrm{i}\omega}{g} \left[\left(\frac{\partial \phi_{d1}^{(1)}}{\partial r} \right)^2 + \left(\frac{\partial \phi_{d1}^{(1)}}{r \partial \theta} \right)^2 \right] \\ & + \frac{2\mathrm{i}\omega}{g} \left[\frac{\partial \phi_i^{(1)}}{\partial r} \frac{\partial \phi_{d1}^{(1)}}{\partial r} + \frac{\partial \phi_{d1}^{(1)}}{r \partial \theta} \frac{\partial \phi_i^{(1)}}{r \partial \theta} \right] \Bigg\} |_{z=0} . \end{aligned} \tag{2.31}$$

It is convenient to express each $\phi_{d1,j}^{(2)}$ $(j = 1, 2, 3)$ in the following general form:

$$\phi_{d1,j}^{(2)} = w_j(r, \theta, z) + \sum_{n=0}^{\infty} \epsilon_n \cos(n\theta) \sum_{m=0}^{\infty} W_{mn,j}(k_m r) Z_m(k_m, z). \tag{2.32}$$

$w_j(r, \theta, z)$ are known functions corresponding to the jth component, which is defined as

$$w_j(r, \theta, z) = \begin{cases} 0, & j = 1, 2, \\ \dfrac{\cosh(k(z+h))}{\nu \cosh(kh)} q(r, \theta), & j = 3. \end{cases} \tag{2.33}$$

$W_{mn,j}$ are functions to be determined and the $Z_m(k_m, z)$ are in each case eigenfunctions defined in (2.15) and (2.16). Now, however, the wavenumbers k_0, k_m ($m = 1, 2, \cdots$) are the real roots of the dispersion equations

$$k_0 \tanh(k_0 h) = 4v, \quad k_m \tan(k_m h) = -4v.$$

We also specify the radiation condition at $r \to \infty$ which is to be satisfied by each unknown function $W_{mn,j}(k_m r)$ as

$$r^{1/2}\left[\frac{\partial W_{mn,j}(k_m r)}{\partial r} - k_m i W_{mn,j}(k_m r)\right] = 0. \tag{2.34}$$

2.3.1. *Second-order 'free wave' component* $\phi^{(2)}_{d1,1}$

The boundary condition at $r = a$ for $\phi^{(2)}_{d1,1}$ is taken as

$$\frac{\partial \phi^{(2)}_{d1,1}}{\partial r} = -\frac{\partial \phi^{(2)}_{i}}{\partial r}, \quad -h \leqslant z \leqslant 0. \tag{2.35}$$

This condition is identical to that for a bottom-seated vertical circular cylinder of height h. Therefore $\phi^{(2)}_{d1,1}$ can be readily written as (e.g. Eatock Taylor & Huang, 1996):

$$\phi^{(2)}_{d1,1} = \sum_{n=0}^{\infty} \epsilon_n \cos(n\theta) \sum_{m=0}^{\infty} \left\{ Q_n \alpha_m \frac{U_n(k_m r)}{U_n'(k_m a)} Z_m(k_m, z) \right\}, \tag{2.36}$$

$$Q_n = \frac{3iA^2\omega}{8} \frac{2kJ_n'(2ka)}{\sinh^4(kh)}, \tag{2.37}$$

where

$$\alpha_0 = \frac{2k \sinh(2kh) + 4v \cosh(2kh)}{4k^2 - k_0^2}, \quad \alpha_m = \frac{2k \sinh(2kh) - 4v \cosh(2kh)}{4k^2 + k_m^2}.$$

$U_n(k_m r)$ is the function defined in (2.14). We see that $\phi^{(2)}_{d1,1}$ has satisfied the governing equation and all the specified boundary conditions.

2.3.2. *Second-order 'locked wave' component* $\phi^{(2)}_{d1,3}$

Based on the theory developed by Eatock Taylor & Huang (1996), a general expression for a particular solution to the second-order wave diffraction by an axisymmetric structure can be written as

$$\phi^{(2)}_{d1,3}(r, \theta, z) = w_3(r, \theta, z) + \sum_{n=0}^{\infty} \sum_{m=0}^{\infty} \epsilon_n R_{mn}(r) Z_m(k_m, z) \cos(n\theta), \tag{2.38}$$

where the first term on the right-hand side is defined in (2.33); $Z_m(k_m, z)$ are eigenfunctions defined in (2.15) and (2.16); and $R_{mn}(r)$ are the functions identified as $W_{mn,3}$ in (2.32), yet to be obtained. κ satisfies the dispersion equation

$$\kappa \tanh(\kappa h) = 5v. \tag{2.39}$$

The above solution for $\phi^{(2)}_{d1,3}$ is defined in the region $a \leqslant r < +\infty$, $0 \leqslant \theta \leqslant 2\pi$, $-h \leqslant z \leqslant 0$. It is clear that $\phi^{(2)}_{d1,3}$ has exactly satisfied the inhomogeneous free-surface condition and the sea-bottom condition. Naturally, $\phi^{(2)}_{d1,3}$ is requried to satisfy

Laplace's equation. This leads to

$$\sum_{m=0}^{\infty}\left[\frac{\mathrm{d}^2R_{mn}}{\mathrm{d}r^2}+\frac{1}{r}\frac{\mathrm{d}R_{mn}}{\mathrm{d}r}+\left(\pm k_m^2-\frac{n^2}{r^2}\right)R_{mn}\right]Z_m(z)+\chi_n(r,z)=0, \tag{2.40}$$

where

$$\chi_n(r,z)=\left[\frac{\mathrm{d}^2q_n}{\mathrm{d}r^2}+\frac{1}{r}\frac{\mathrm{d}q_n}{\mathrm{d}r}+\left(\kappa^2-\frac{n^2}{r^2}\right)q_n\right]\frac{\cosh(\kappa(z+d))}{v\cosh(\kappa d)}. \tag{2.41}$$

$q_n(r)$ is the nth Fourier mode of the forcing function $q(r,\theta)$, and the $\pm$ is taken to be $+$ when $m=0$ and $-$ when $m>0$. Again, using the eigenfunction-expansion technique in the z-direction, we obtain

$$\frac{\mathrm{d}^2R_{mn}}{\mathrm{d}r^2}+\frac{1}{r}\frac{\mathrm{d}R_{mn}}{\mathrm{d}r}+\left(\pm k_m^2-\frac{n^2}{r^2}\right)R_{mn}+A_m\left[\frac{\mathrm{d}^2q_n}{\mathrm{d}r^2}+\frac{1}{r}\frac{\mathrm{d}q_n}{\mathrm{d}r}+\left(\kappa^2-\frac{n^2}{r^2}\right)q_n\right]=0, \tag{2.42}$$

where

$$A_m=\int_0^d\frac{\cosh\kappa(z+d)}{v\cosh(\kappa d)}Z_m(z)\mathrm{d}z. \tag{2.43}$$

We now let $\Phi_{mn}(r)=R_{mn}+A_mq_n(r)$. Equation (2.42) can be rearranged into an inhomogeneous Sturm–Liouville ordinary equation of the form

$$Ł(y(x))+\phi(x)=0 \tag{2.44}$$

with

$$Ł=\frac{\mathrm{d}}{\mathrm{d}x}\left(p\frac{\mathrm{d}}{\mathrm{d}x}\right)+q=p(x)\frac{\mathrm{d}^2}{\mathrm{d}x^2}+\frac{\mathrm{d}p}{\mathrm{d}x}\frac{\mathrm{d}}{\mathrm{d}x}+q(x). \tag{2.45}$$

In the present case,

$$y=\Phi_{mn}(r),\quad p=r,\quad q=\pm\left(k_m^2\mp\frac{n^2}{r^2}\right)r,$$

$$\phi=A_mq_n(\kappa^2\mp k_m^2)r.$$

The above Sturm–Liouville equation, subject to the boundary conditions specified at $r=a$ and $r=\infty$, can be solved exactly by using a one-dimensional Green's function. This leads to

$$\phi^{(2)}_{d1,3}(r,\theta,z)=\sum_{n=0}^{\infty}\epsilon_n\cos(n\theta)\left\{\sum_{m=0}^{\infty}Z_m(k_m,0)Z_m(k_m,z)\int_a^{\infty}\xi q_n(\xi)G_{mn}(r,\xi)\mathrm{d}\xi\right\}, \tag{2.46}$$

where the Green's function $G_{mn}(r,\xi)$ is given by:

$$G_{0n}(r,\xi)=\begin{cases}\mathrm{i}\pi H_n(k_0\xi)[J_n(k_0r)-\beta_0(n)H_n(k_0r)]/2, & r<\xi,\\ \mathrm{i}\pi H_n(k_0r)[J_n(k_0\xi)-\beta_0(n)H_n(k_0\xi)]/2, & r>\xi,\end{cases} \tag{2.47}$$

$$G_{mn}(r,\xi)=\begin{cases}K_n(k_m\xi)[I_n(k_mr)-\beta_m(n)K_n(k_mr)], & r<\xi,\\ K_n(k_mr)[I_n(k_m\xi)-\beta_m(n)K_n(k_m\xi)], & r>\xi,\end{cases} \tag{2.48}$$

with

$$\beta_0(n)=J_n'(k_0a)/H_n'(k_0a),\quad \beta_m(n)=I_n'(k_ma)/K_n'(k_ma).$$

2.3.3. *Second-order 'free wave' component* $\phi^{(2)}_{d1,2}$

The expressions for $\phi^{(2)}_{d1,2}(r,\theta,z)$ in the exterior region and the total second-order potential in the interior region $\phi^{(2)}_2(r,\theta,z)$ have the forms

$$\phi^{(2)}_{d1,2}(r,\theta,z) = \sum_{n=0}^{\infty} \epsilon_n \cos(n\theta) \left\{ \sum_{m=0}^{\infty} B^{(2)}_{mn} \frac{U_n(k_m r)}{U'_n(k_m a)} Z_m(k_m, z) \right\}, \tag{2.49}$$

$$\phi^{(2)}_2(r,\theta,z) = \sum_{n=0}^{\infty} \epsilon_n \cos(n\theta) \left\{ \sum_{m=0}^{\infty} A^{(2)}_{mn} V_n(\lambda_m r) \cos(\lambda_m(z+h)) \right\}, \tag{2.50}$$

where λ_m and $V_n(\lambda_m r)$ are defined in §2.2.

Using the continuity conditions (2.8) and (2.9), we can obtain

$$\sum_{m=0}^{\infty} B^{(2)}_{mn} k_m Z_m(k_m, z) = \begin{cases} \displaystyle\sum_{m=0}^{\infty} A^{(2)}_{mn} \frac{\partial V_n(\lambda_m a)}{\partial r} \cos\lambda_m(z+h), & -h \leqslant z \leqslant -b, \\ 0, & -b < z \leqslant 0, \end{cases} \tag{2.51}$$

$$\sum_{m=0}^{\infty} A^{(2)}_{mn} V_n(\lambda_m a) \cos(\lambda_m(z+h)) = \phi^{(2)}_{0n}(a,z) + \sum_{j=0}^{\infty} B^{(2)}_{jn} \frac{U_n(k_j a)}{U'_n(k_j a)} Z_j(k_j, z), \tag{2.52}$$

where

$$\phi^{(2)}_{0n}(a,z) = (\phi^{(2)}_i + \phi^{(2)}_{d1,1} + \phi^{(2)}_{d1,3})_n, \tag{2.53}$$

subscript n denoting the nth Fourier mode of the corresponding second-order potential components. It can be shown that $\phi^{(2)}_{0n}$ corresponds to the complete second-order potential for a bottom-seated vertical circular cylinder, described in Chau & Eatock Taylor (1992).

2.4. *Solution for the coefficients*

Using the above conditions and the eigenfunction expansion method, we can derive expressions for $A^{(2)}_{mn}$ and $B^{(2)}_{mn}$ in a similar manner to the solution for the coefficients of the first-order potentials. Analogous to (2.21) and (2.22) we obtain

$$\{B^{(2)}_n\} = [C^{(2)}_n]\{A^{(2)}_n\}, \tag{2.54}$$

$$\{A^{(2)}_n\} = [D^{(2)}_n]\{B^{(2)}_n\} + \{E^{(2)}_n\}, \tag{2.55}$$

where

$$\{B^{(2)}_n\} = (B^{(2)}_{mn}),\ \{A^{(2)}_n\} = (A^{(2)}_{mn}), \quad m = 0,1,2,\cdots, \quad n = 0,1,2,\cdots, \tag{2.56}$$

$$C^{(2)}_n(j,m) = \frac{V'_n(\lambda_m a)}{k_m h} \int_{-h}^{-b} \cos(\lambda_m(z+h)) Z_j(k_j, z)\mathrm{d}z, \tag{2.57}$$

$$D^{(2)}_n(m,j) = \frac{2}{d} \frac{U_n(k_j a)}{U'_n(k_j a)} \int_{-h}^{-b} \cos(\lambda_m(z+h)) Z_j(k_j, z)\mathrm{d}z, \tag{2.58}$$

$$E^{(2)}_n(m) = \int_{-h}^{-b} \phi^{(2)}_{0n}(a,z) \cos(\lambda_m(z+h))\mathrm{d}z. \tag{2.59}$$

Each of these definitions holds for $j = 0,1,\cdots$ and $m = 0,1,\cdots$ with $\lambda_0 = 0$, though in the numerical implementation the ranges are of course truncated. More detailed expressions for $[D^{(2)}_n]$, $[C^{(2)}_n]$ and $\{E^{(2)}_n\}$ are given in Appendix B.

3. Forces, moments and free-surface elevation

3.1. *First-order forces*

The first-order pressure is

$$p^{(1)}(r,\theta,z,t) = \mathrm{Re}\{\mathrm{i}\rho\omega\phi_1^{(1)}(r,\theta,z)\mathrm{e}^{-\mathrm{i}\omega t}\}. \tag{3.1}$$

The first-order wave elevation in the exterior region is

$$\eta^{(1)}(r,\theta,t) = \mathrm{Re}\left\{\frac{\mathrm{i}\omega}{g}\phi_1^{(1)}(r,\theta,0)\mathrm{e}^{-\mathrm{i}\omega t}\right\}. \tag{3.2}$$

The first-order surge force is

$$F_x^{(1)}(t) = \mathrm{Re}\left\{\pi\mathrm{i}\rho\omega a^2\mathrm{e}^{-\mathrm{i}\omega t}\left[\frac{\sinh(kh)-\sinh(kd)}{ka}\left(\frac{P_1(ka)}{\cosh(kh)}+\frac{B_{01}^{(1)}H_1(ka)}{\gamma_0^{1/2}H_1'(ka)}\right)\right.\right.$$
$$\left.\left.+\sum_{j=1}^{\infty}\frac{B_{j1}^{(1)}}{[\gamma_j(m_j)]^{1/2}}\frac{K_1(m_ja)}{K_1'(m_ja)}\frac{\sin(m_jh)-\sin(m_jd)}{m_ja}\right]\right\}. \tag{3.3}$$

The first-order vertical force is

$$F_z^{(1)}(t) = \mathrm{Re}\left\{\mathrm{i}\omega\rho\mathrm{e}^{-\mathrm{i}\omega t}\int_0^{2\pi}\int_0^a \phi_2^{(1)}(r,\theta,-b)r\,\mathrm{d}r\,\mathrm{d}\theta\right\}. \tag{3.4}$$

Upon substituting the expression for $\phi_2^{(1)}$ into (3.4), we obtain

$$F_z^{(1)}(t) = \mathrm{Re}\left\{\mathrm{i}\omega\rho\pi a^2\mathrm{e}^{-\mathrm{i}\omega t}\left[\frac{A_{00}^{(1)}}{2}+\sum_{m=1}^{\infty}\frac{A_{m0}^{(1)}(-1)^mI_1(\lambda_ma)}{\lambda_maI_0(\lambda_ma)}\right]\right\}. \tag{3.5}$$

3.2. *Second-order forces*

The second-order forces can be decomposed into several components (see, for example, Eatock Taylor & Hung 1987; Kim & Yue 1989), namely the second-order mean force, the force due to the quadratic contribution of the first-order potential and the force due to the contribution of the time-varying second-order potential. Explicit expressions for various second-order components are given in the following subsections.

3.2.1. *Mean second-order forces and moments*

The mean surge force is

$$\overline{F}_x^{(2)} = \mathrm{Re}\left\{-\frac{\rho}{4}\int_{S_B}|\nabla\phi^{(1)}|^2n_j\,\mathrm{d}s+\frac{\rho\omega^2}{4g}\int_{W_0}|\phi^{(1)}|^2n_j\,\mathrm{d}l\right\}$$
$$= \mathrm{Re}\{\overline{F}_{x1}^{(2)}+\overline{F}_{x2}^{(2)}\}, \tag{3.6}$$

where S_B denotes the body surface and W_0 denotes the waterline. We obtain

$$\overline{F}_{x1}^{(2)} = -\pi\rho a\int_{-b}^{0}\sum_{n=0}^{\infty}\left\{\varphi(n,z)\varphi^*(n+1,z)\frac{n(n+1)}{a^2}+\frac{\mathrm{d}\varphi(n,z)}{\mathrm{d}z}\frac{\mathrm{d}\varphi^*(n+1,z)}{\mathrm{d}z}\right\}\mathrm{d}z, \tag{3.7}$$

where

$$\varphi(n,z) = P_n(ka)\frac{\cosh k(z+h)}{\cosh kh}+\sum_{j=0}^{\infty}B_{jn}^{(1)}\frac{U_n(m_ja)}{\epsilon_nU_n'(m_ja)}Z_j(m_j,z), \tag{3.8}$$

and

$$\overline{F}_{x2}^{(2)} = \frac{\pi\rho a\omega^2}{g}\sum_{n=0}^{\infty}\varphi(n,0)\varphi^*(n+1,0). \tag{3.9}$$

The pitch moment about an axis through the base of the cylinder ($z=-b$) is

$$\overline{M}_y^{(2)} = \mathrm{Re}\left\{-\pi\rho a\int_{-b}^{0}\sum_{n=0}^{\infty}\left[\varphi(n,z)\varphi^*(n+1,z)\frac{n(n+1)}{a^2} + \frac{\mathrm{d}\varphi(n,z)}{\mathrm{d}z}\frac{\mathrm{d}\varphi^*(n+1,z)}{\mathrm{d}z}\right](b+z)\mathrm{d}z + \overline{F}_{x2}^{(2)}b\right\}. \tag{3.10}$$

The heave force is

$$\overline{F}_z^{(2)} = \mathrm{Re}\left\{-\frac{\pi\rho}{4}\int_0^a\sum_{n=0}^{\infty}r\left[\psi(n,r)\psi^*(n,r)\frac{n^2}{r^2} + \frac{\mathrm{d}\psi(n,r)}{\mathrm{d}r}\frac{\mathrm{d}\psi^*(n,r)}{\mathrm{d}r}\right]\mathrm{d}r\right\}, \tag{3.11}$$

where

$$\psi(n,r) = \frac{A_{0n}^{(1)}}{2}\left(\frac{r}{a}\right)^n + \sum_{m=1}^{\infty}\frac{A_{mn}^{(1)}(-1)^m I_n(\lambda_m r)}{I_n(\lambda_m a)}. \tag{3.12}$$

3.2.2. *Second-order quadratic forces and moments*

The quadratic component of the surge force is

$$\begin{aligned} F_{xq}^{(2)} &= \mathrm{Re}\left\{-\frac{\rho}{4}\int_{S_B}|\nabla\phi^{(1)}|^2 n_j\mathrm{d}s - \frac{\rho\omega^2}{4g}\int_{W_0}|\phi^{(1)}|^2 n_j\mathrm{d}l\right\} \\ &= \mathrm{Re}\{(F_{xq,1}^{(2)} + F_{xq,2}^{(2)})\mathrm{e}^{-2\mathrm{i}\omega t}\}, \end{aligned} \tag{3.13}$$

where

$$F_{xq,1}^{(2)} = -\pi\rho a\int_{-b}^{0}\sum_{n=0}^{\infty}\left\{\frac{n(n+1)}{a^2}\varphi(n,z)\varphi(n+1,z) + \frac{\mathrm{d}\varphi(n,z)}{\mathrm{d}z}\frac{\mathrm{d}\varphi(n+1,z)}{\mathrm{d}z}\right\}\mathrm{d}z, \tag{3.14}$$

$$F_{xq,2}^{(2)} = -\frac{\pi\rho a\omega^2}{g}\sum_{n=0}^{\infty}\varphi(n,0)\varphi(n+1,0). \tag{3.15}$$

The quadratic component of the pitch moment is

$$M_{qy}^{(2)} = \mathrm{Re}\{(M_{qy,1}^{(2)} + F_{qx,2}^{(2)}b)\mathrm{e}^{-2\mathrm{i}\omega t}\}, \tag{3.16}$$

where

$$M_{qy,1}^{(2)} = -\pi\rho a\int_{-b}^{0}\sum_{n=0}^{\infty}\left[\varphi(n,z)\varphi(n+1,z)\frac{n(n+1)}{a^2} + \frac{\mathrm{d}\varphi(n,z)}{\mathrm{d}z}\frac{\mathrm{d}\varphi(n+1,z)}{\mathrm{d}z}\right](b+z)\}\mathrm{d}z. \tag{3.17}$$

The quadratic component of the heave force is

$$F_{zq}^{(2)} = \mathrm{Re}\left\{-\frac{\pi\rho}{4}\int_0^a\sum_{n=0}^{\infty}r\left[\psi^2(n,r)\frac{n^2}{r^2} + \left(\frac{\mathrm{d}\psi(n,r)}{\mathrm{d}r}\right)^2\right]\mathrm{d}r\right\}. \tag{3.18}$$

3.2.3. *Forces and moments due to second-order potential*

The contribution of $\phi^{(2)}$ to the surge force is

$$F_{xd}^{(2)} = \mathrm{Re}\left\{2\mathrm{i}\omega\rho\pi a\mathrm{e}^{-2\mathrm{i}\omega t}\int_{-b}^{0}\left[\phi_{01}^{(2)}(a,z)+\sum_{m=0}^{\infty}B_{m1}^{(2)}Z_m(k_m,z)\frac{U_1(k_m a)}{U_1'(k_m a)}\right]\mathrm{d}z\right\}. \tag{3.19}$$

The pitch moment contribution is

$$M_{yd}^{(2)} = \mathrm{Re}\left\{2\mathrm{i}\omega\rho\pi a\mathrm{e}^{-2\mathrm{i}\omega t}\int_{-b}^{0}\left[\phi_{01}^{(2)}(a,z)+\sum_{m=0}^{\infty}B_{m1}^{(2)}Z_m(k_m,z)\frac{U_1(k_m a)}{U_1'(k_m a)}\right](b+z)\mathrm{d}z\right\}. \tag{3.20}$$

The heave force contribution is

$$F_{zd}^{(2)}(t) = \mathrm{Re}\left\{2\mathrm{i}\omega\rho\pi a^2\mathrm{e}^{-2\mathrm{i}\omega t}\left[\frac{A_{00}^{(2)}}{2}+\sum_{m=1}^{\infty}\frac{A_{m0}^{(2)}(-1)^m I_1(\lambda_m a)}{\lambda_m a I_0(\lambda_m a)}\right]\right\}. \tag{3.21}$$

3.3. *Free-surface elevation*

The second-order free-surface elevation ζ can also be decomposed into three parts: the second-order mean component, the second-order quadratic component and the component due to the time-varying second-order potential. We therefore write the elevation as follows:

$$\zeta^{(2)}(r,\theta,t) = \mathrm{Re}\{[\eta_q^{(2)}+\eta_d^{(2)}]\mathrm{e}^{-2\mathrm{i}\omega t}+\bar{\eta}^{(2)}\}, \tag{3.22}$$

where

$$\eta_q^{(2)}(r,\theta) = \left\{-\frac{1}{4g}(\nabla\phi_1^{(1)})^2-\frac{\omega^2}{2g^2}\phi_1^{(1)}\frac{\partial\phi_1^{(1)}}{\partial z}\right\}\Bigg|_{z=0}, \tag{3.23}$$

$$\bar{\eta}^{(2)}(r,\theta) = \left\{-\frac{1}{4g}|\nabla\phi_1^{(1)}|^2+\frac{\omega^2}{2g^2}\phi_1^{(1)}\frac{\partial\phi_1^{(1)*}}{\partial z}\right\}\Bigg|_{z=0}, \tag{3.24}$$

$$\eta_d^{(2)}(r,\theta) = \frac{2\mathrm{i}\omega}{g}[\phi_{d1}^{(2)}+\phi_i^{(2)}]|_{z=0}. \tag{3.25}$$

These are the complete expressions based on the exact solution of the boundary value problem.

4. Approximate solution to second-order potentials and forces

Many ocean structures such as tension leg platforms (TLPs) have a rather complicated geometry, which makes the corresponding nonlinear hydrodynamic analysis difficult. At second order, the boundary-element approach is usually expensive. In the case of multi-column structures such as TLPs, however, we can investigate whether under relevant practical conditions the dominating contribution to the diffracted potential, either first or second order, comes from the upper part of the structure consisting of the vertical cylinders. Great advantage could be obtained by exploiting such an assumption. In this section, we give an approximate solution to the second-order potential and corresponding forces on a truncated circular cylinder, aimed at providing an efficient approach to nonlinear hydrodynamic analysis of complicated structures such as TLPs.

The basic assumption here is that for 'deep draught' structures, the lower part of the structure will make little contribution to the diffracted potential. In effect, we assume that the contributions $\phi^{(1)}_{dI,2}$ in (2.11) and $\phi^{(2)}_{dI,2}$ in (2.29) are negligible. As is shown in the numerical results of §5, this approximation is reasonable even for structures with moderate draught. By neglecting the contribution of the lower part, we assume that the diffracted potential induced by a truncated cylinder is the same as that for a bottom-seated surface-piercing cylinder with the same diameter and in the same water depth. Hence, in the exterior region in the truncated cylinder problem, the total second-order potential is approximated by

$$\phi^{(2)}(r,\theta,z) = \sum_{n=0}^{\infty} \epsilon_n \cos(n\theta) \left\{ -\frac{3iA^2\omega}{8} \frac{\cosh(2k(z+h))}{\sinh^4(kh)} i^n J_n(2kr) + \sum_{m=0}^{\infty} \left[Z_m(k_m,0) \int_a^{\infty} \xi q_n(\xi) G_{mn}(r,\xi) d\xi + Q_n \alpha_m \frac{U_n(k_m r)}{U_n'(k_m a)} \right] Z_m(k_m,z) \right\}. \tag{4.1}$$

Expressions for Q_n and α_m are given in §2.3.1.

Since this solution corresponds to the exterior region outside the vertical cylinder, we cannot directly obtain the second-order vertical force on the cylinder. To do so we extend this solution to the interior region where the total second-order potential only consists of the free-wave component. The form of the potential in the interior region is given by (2.50). By matching that expression with (2.27), using the continuity condition for the total second-order potential, we obtain a decoupled expression for $\{A_n^{(2)}\}$:

$$\{A_n^{(2)}\} = \{E_n^{(2)}\}. \tag{4.2}$$

The expressions for $E_n^{(2)}$ are given in (2.59) and Appendix B.

It can be seen that the above approximate solution has a very simple form, for which efficient and reliable algorithms now exist (Chau & Eatock Taylor 1992; Eatock Taylor & Huang 1996). Based on these simplifications, analytical expressions for the mean and quadratic components of second-order surge and pitch forces acting on the cylinder are derived and given in Appendix C. These expressions are analogous to those given in Appendix B of Kim & Yue (1989). In their expressions, the integration is carried out over the whole length of the bottom-seated cylinder, while in our expressions only the upper part corresponding to the surface of the truncated cylinder is retained in the integrals. The expressions for second-order dynamic loads due to the contribution of the approximated second-order potential can be obtained from those in (3.19)–(3.21), simply by putting $B_{m1}^{(2)} = 0$, $m = 0, 1, 2, \cdots$.

5. Numerical results and discussion

5.1. *Convergence of the solution*

In order to ensure that the numerical results are reliable, we first test the convergence of the semi-analytical method and the corresponding computer program. There are two parameters which influence the accuracy of the calculation: the number of Fourier modes N and the number of eigen modes M. In our numerical algorithm, N is determined by a truncation-error tolerance, which is set at $\epsilon = 10^{-5}$. Thus for a

	$h/a =$	10.0		15.0		25.0	
$F_x^{(2)}$	$M = 50$	(0.5603,	0.4392)	(0.5537,	0.4573)	(0.5573,	0.4309)
	$M = 100$	(0.5602,	0.4390)	(0.5535,	0.4551)	(0.5585,	0.4321)
	$M = 150$	(0.5602,	0.4389)	(0.5535,	0.4559)	(0.5582,	0.4310)
$F_z^{(2)}$	$M = 50$	(−0.0039,	−0.3822)	(−0.0030,	−0.3865)	(−0.0046,	−0.3816)
	$M = 100$	(−0.0039,	−0.3822)	(−0.0030,	−0.3865)	(−0.0046,	−0.3816)
$M_y^{(2)}$	$M = 50$	(0.3147,	−0.1900)	(0.3159,	−0.1840)	(0.3132,	−0.1924)
	$M = 100$	(0.3147,	−0.1897)	(0.3158,	−0.1857)	(0.3143,	−0.1923)
	$M = 150$	(0.3147,	−0.1894)	(0.3159,	−0.1850)	(0.3141,	−0.1931)

TABLE 1. Convergence of real and imaginary parts (real, imag) of total second-order forces (surge, heave, pitch) for different numbers (M) of eigen modes. Forces and pitch moment (with respect to the cylinder bottom) are normalized by $\rho g a A^2$ and $\rho g a A^2 b$ respectively ($ka = 0.8$, $b/a = 4.0$).

	$ka =$	0.5		1.5		2.5	
$F_x^{(2)}$	$M = 50$	(0.4062,	−0.0337)	(2.4470,	0.4390)	(0.0426,	−3.9426)
	$M = 100$	(0.4062,	−0.0360)	(2.4469,	0.4390)	(0.0426,	−3.9424)
	$M = 200$	(0.4062,	−0.0278)	(2.4469,	0.4390)	(0.0426,	−3.9424)
	$M = 250$	(0.4062,	−0.0275)	(2.4469,	0.4390)	(0.0426,	−3.9424)
$F_z^{(2)}$	$M = 50$	(−0.0580,	−0.2196)	(−0.2456,	−0.1132)	(−0.1503,	0.4045)
	$M = 100$	(−0.0580,	−0.2196)	(−0.2456,	−0.1132)	(−0.1503,	0.4046)
$M_y^{(2)}$	$M = 50$	(0.3073,	−0.4120,)	(1.4527,	0.0935)	(−0.1455,	−2.5346)
	$M = 100$	(0.3073,	−0.4130)	(1.4529,	0.0936)	(−0.1454,	−2.5349)
	$M = 200$	(0.3073,	−0.4123)	(1.4529,	0.0936)	(−0.1454,	−2.5349)
	$M = 250$	(0.3073,	−0.4129)	(1.4529,	0.0936)	(−0.1454,	−2.5349)

TABLE 2. Convergence of real and imaginary parts (real, imag) of total second-order forces (surge, heave, pitch) for different numbers (M) of eigen modes. Forces and pitch moment (with respect to the cylinder bottom) are normalized by $\rho g a A^2$ and $\rho g a A^2 b$ respectively ($h/a = 20$, $b/a = 4.0$).

summation $\sum_{n=0}^{\infty} \psi_n$, N is the smallest value such that

$$\left| \sum_{n=0}^{N+1} \psi_n - \sum_{n=0}^{N} \psi_n \right| \Big/ \left| \sum_{n=0}^{N+1} \psi_n \right| < \epsilon.$$

In general, $N = 12$ is sufficient for most cases. For this reason it is only the influence of M which is examined here. Table 1 illustrates the convergence characteristics for a given ka and varying non-dimensional water depth kh; while table 2 shows the characteristics with respect to variation of ka for a given h/a. In both cases the convergence is satisfactory, and the results show that this has little dependence on either ka or kh. We have also carried out many other computations (not presented here), the results of which confirm that the solution possesses very good convergence characteristics. Even for very deep water ($kh > 20$), $M = 100$ can yield an accuracy higher than 99%, over the entire range of ka which is of interest. We believe that this is because in our solution both first-order and second-order potentials are expressed as sums of components corresponding to a bottom-seated cylinder, with the same radius and water depth, and a correction term due to the truncation of the cylinder. The contribution of the correction term to the velocity potential on the free surface is small in comparison with the leading term, yielding good computational features.

	$ka =$	0.8	1.2	2.0
$F_{xq}^{(2)}$	Semi-analytical	(−0.4425, −1.4746)	(−1.4356, −0.7970)	(−1.3530, 0.7652)
	BEM results	(−0.4452, −1.4709)	(−1.4334, −0.8024)	(−1.3629, 0.7606)
$F_{xd}^{(2)}$	Semi-analytical	(1.0144, 1.9740)	(3.0406, 1.6594)	(3.9052, −2.4883)
	BEM results	(1.0261, 1.9702)	(3.0451, 1.6570)	(3.8702, −2.4750)
$F_{x}^{(2)}$	Semi-analytical	(0.5719, 0.4994)	(1.6050, 0.8629)	(2.5529, −1.7233)
	BEM results	(0.5808, 0.4991)	(1.6116, 0.8552)	(2.5071, −1.7144)
$F_{z}^{(2)}$	Semi-analytical	(−0.0020, −0.4047)	(−0.0690, −0.3319)	(−0.4941, 0.2319)
	BEM results	(−0.0026, −0.4084)	(−0.0695, −0.3347)	(−0.4960, 0.2331)

TABLE 3. Components of second-order surge and heave forces on a truncated circular cylinder, normalized by $\rho g a A^2$ ($b/a = 4$, $h/a = 10.0$).

	$kb =$	1.2	1.5	2.0
$F_{x}^{(2)}$	Exact	(0.4535, −0.1708)	(0.4138, −0.1033)	(0.4062, −0.0358)
$F_{x}^{(2)}$	Approx.	(0.4208, −0.2799)	(0.3736, −0.1379)	(0.4018, −0.0230)
$\lvert F_{x}^{(2)}\rvert$	Exact	0.4843	0.4265	0.4077
$\lvert F_{x}^{(2)}\rvert$	Approx.	0.5054	0.3982	0.4025
$F_{z}^{(2)}$	Exact	(−0.0986, −0.1683)	(−0.0988, −0.2684)	(−0.0582, −0.2195)
$F_{z}^{(2)}$	Approx.	(−0.1084, −0.1775)	(−0.1101, −0.2858)	(−0.0993, −0.2198)
$\lvert F_{z}^{(2)}\rvert$	Exact	0.1951	0.2860	0.2271
$\lvert F_{z}^{(2)}\rvert$	Approx.	0.2080	0.3063	0.2273
$M_{y}^{(2)}$	Exact	(0.3445, −0.5021)	(0.3053, −0.5018)	(0.3073, −0.4137)
$M_{y}^{(2)}$	Approx.	(0.3183, −0.5576)	(0.2682, −0.5175)	(0.2983, −0.4073)
$\lvert M_{y}^{(2)}\rvert$	Exact	0.6089	0.5874	0.5153
$\lvert M_{y}^{(2)}\rvert$	Approx.	0.6420	0.5828	0.5049

TABLE 4. Comparison of approximate solution with exact solution for second-order mean force in surge and total time-varying second-order forces in surge, heave, and pitch. Forces and pitch moment are normalized by $\rho g a A^2$ and $\rho g a A^2 b$ respectively ($ka = 0.5$, $h/a = 20.0$).

5.2. *Comparison with results from the boundary-element method*

In order to validate the algorithm, we compare the semi-analytical results for components of second-order surge and heave forces on a truncated cylinder ($b/a = 4$, $h/a = 10.0$) with numerical results obtained by using the computer program DIFFRACT based on a higher-order boundary-element method (Eatock Taylor & Chau 1992). Table 3 gives the real and imaginary parts (real, imag) for these results for three different frequencies. For the results from the boundary element method (designated BEM), 360 quadratic elements were used in each quadrant ($N_c \times N_z = 10 \times 15$ elements on the surface of the cylinder, $N_c \times N_r = 10 \times 15$ elements on the water plane area, and $N_c \times N_R = 10 \times 6$ elements on the cylinder bottom, N_c N_r N_z N_R being the number of elements in the circumferential direction, in the radial direction on the free surface, in the vertical direction along the cylinder, and in the radial direction on the bottom surface respectively). Advantage was taken of the two planes of symmetry. It can be seen that good agreement is obtained between the semi-analytical and the BEM results.

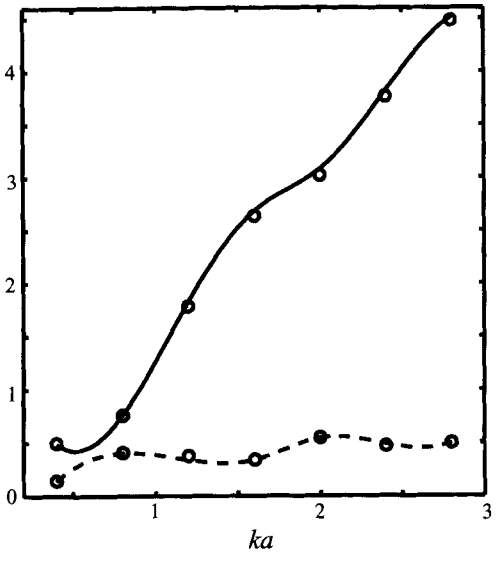

FIGURE 2. Variation with ka of magnitudes of total dimensionless time-varying second-order surge (——) and heave (– – –) forces; o symbol shows BEM results based on the mesh described in table 3 ($h/a = 10.0$, $b/a = 4.0$).

5.3. *Comparison of results from exact and approximate semi-analytical solutions*

In order to assess the validity of the approximate solution given in §4, we tabulate a set of results from the exact method and the approximate method. The total time-varying second-order forces in surge, heave and pitch for three different dimensionless draughts kb are given in table 4. This shows that the accuracy of the approximate solution is satisfactory even for a moderate draught. The relative error in magnitudes arising from the approximation is generally less than 7% for $kb \geqslant 1.2$. More comparisons of the exact solution with the approximate solution are given in §§5.4 and 5.5.

5.4. *Results for second-order forces and moments under various conditions*

We can now consider the effects of different factors on the total time-varying second-order forces and the moment. Figure 2 shows the variation with ka of the magnitudes of the forces in surge and heave for a particular configuration. For comparison, also presented are the results obtained by using the computer program DIFFRACT. It is seen that the surge force incresases quickly with increasing ka. The variation of heave force, however, is comparatively small.

Figure 3(a) shows the influence of non-dimensional water depth kh on these forces and the moment. Results from the semi-analytical solution, shown as lines, are compared with results obtained by using the approximate method, shown as plotting symbols. The agreement in heave is very good over the whole range of kh considered here. For $kh \geqslant 5.0$, good agreement is also reached for surge and pitch. It is also seen from the figure that the influence of kh on the second-order forces is fairly small.

Results showing the variation with non-dimensional draught kb are given in figure 3(b), with the same comparisons as in figure 3(a). We see that for $kb > 1.2$, the agreement between exact and approximate solutions is very good. By comparing figures 3(a) and 3(b), we find that the influence of kb on the second-order forces is much stronger than that of kh, especially in the case of the heave force.

Figure 3(c) illustrates the comparison between the exact and approximate solutions

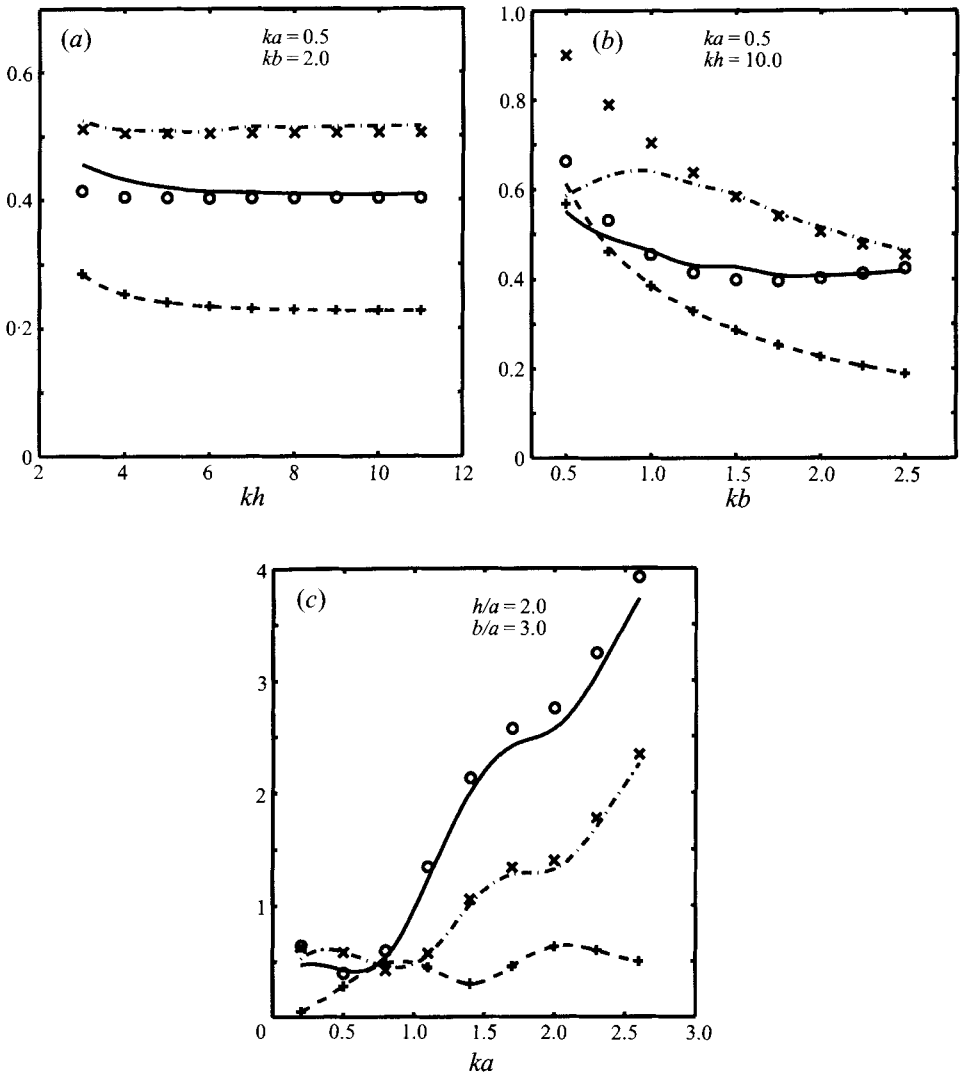

FIGURE 3. Variation with (*a*) kh, (*b*) kb and (*c*) ka of magnitudes of total dimensionless time-varying second-order forces and moment: ——, surge force; — — —, heave force; — · — · —, pitch moment. o, ×, +, denote results calculated using the approximate method.

for the second-order forces and moment over a range of ka while keeping h/a and b/a constant ($h/a = 20.0, b/a = 3.0$). Again, the agreement in heave is always very good. For these specific values of h/a and b/a, when $ka > 0.5$, results from exact and approximate solutions are very close to each other for all the three force components.

The vertical distributions of the magnitude of the first-order and second-order surge forces per unit length are shown in figure 4 for $ka = 0.4$ and $ka = 1.0$, with $h/a = 20$. Results for a bottom-seated circular cylinder with the same ka and kh are also presented for comparison. In the case of $ka = 1.0$ and $kh = 20.0$, both first-order and second-order surge forces (per unit length) are very close for a truncated cylinder and a bottom-seated cylinder. In the case of $ka = 0.4$ and $kh = 8$, there is a significant difference in the first-order surge force between the two cylinders at the position near the bottom of the truncated cylinder ($z = -b$), showing the effect of

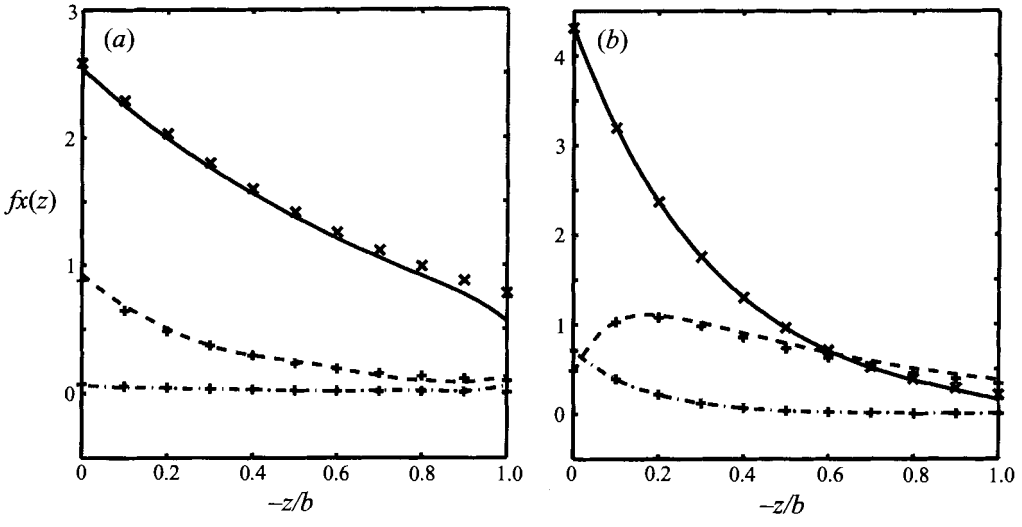

FIGURE 4. Variation with z/b of magnitudes of first- and second-order surge forces per unit length of the cylinder surface: (*a*) $ka = 0.4, kh = 8$; (*b*) $ka = 1.0$, $kh = 20.0$. ×, + denote results for a bottom-seated cylinder with the same ka and kh ($b/a = 3.0$ $h/a = 20.0$).

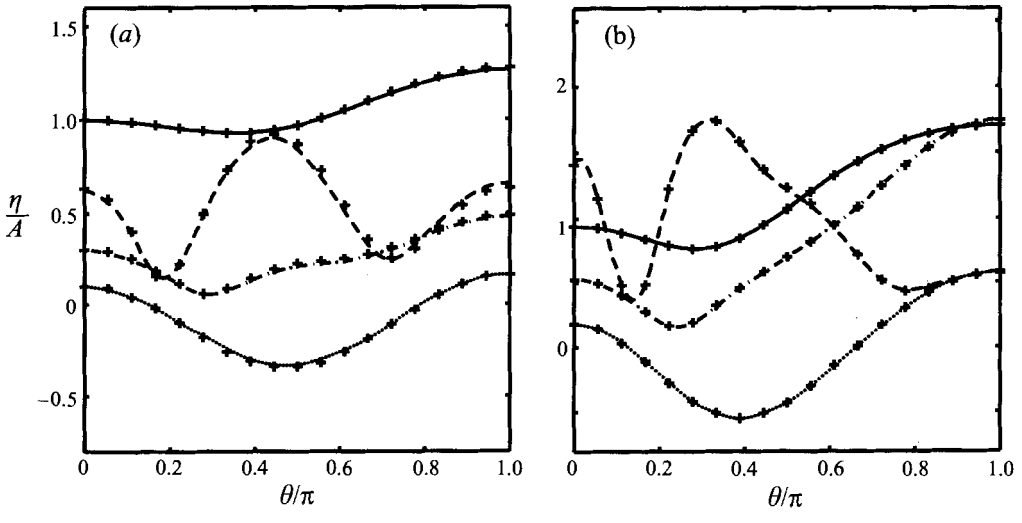

FIGURE 5. Magnitudes of first and second-order free-surface elevation on the waterline for two different ka. ——, $|\eta^{(1)}/A|$; – – –, $|\eta^{(2)}a/A^2|$; — · — · —, $|\eta_q^{(2)}a/A^2|$; ·····, $\bar{\eta}^{(2)}a/A^2$. Symbols denote results for a bottom-seated cylinder with the same ka and kh. $\theta = 180$ corresponds to the side facing the incoming wave. (*a*) $ka = 0.4$; (*b*) $ka = 0.8$.

the boundary condition on the cylinder bottom. For the time-varying second-order force, the biggest difference occurs near the free surface. Over most of the depth of the truncated cylinder, the difference with the surge force distribution on the bottom-seated cylinder is very small. For the second-order mean force, there is no significant difference along the whole length of the cylinder.

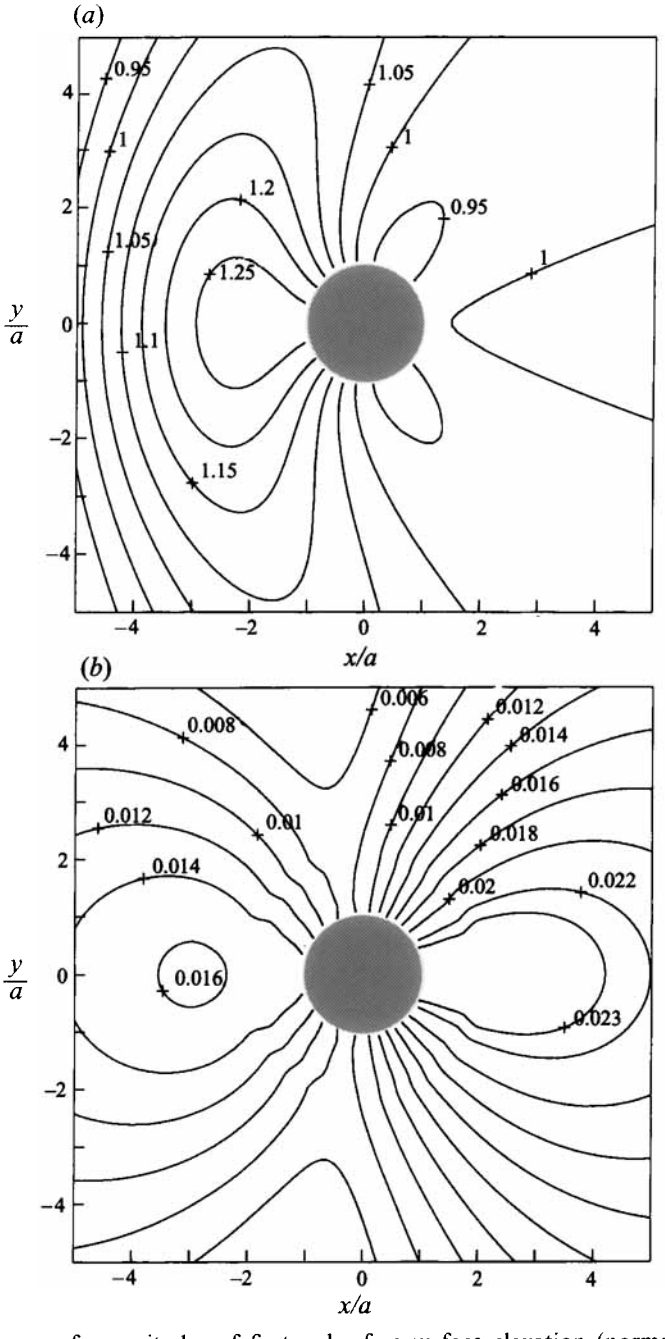

FIGURE 6. Contours of magnitudes of first-order free-surface elevation (normalized by the wave amplitude A) for $ka = 0.4$, $kh = 8.0$. (*a*) Truncated cylinder with $b/a = 3.0$; (*b*) difference in amplitudes between the truncated cylinder and a bottom-seated cylinder in the same depth of water. Wave direction is from left to right.

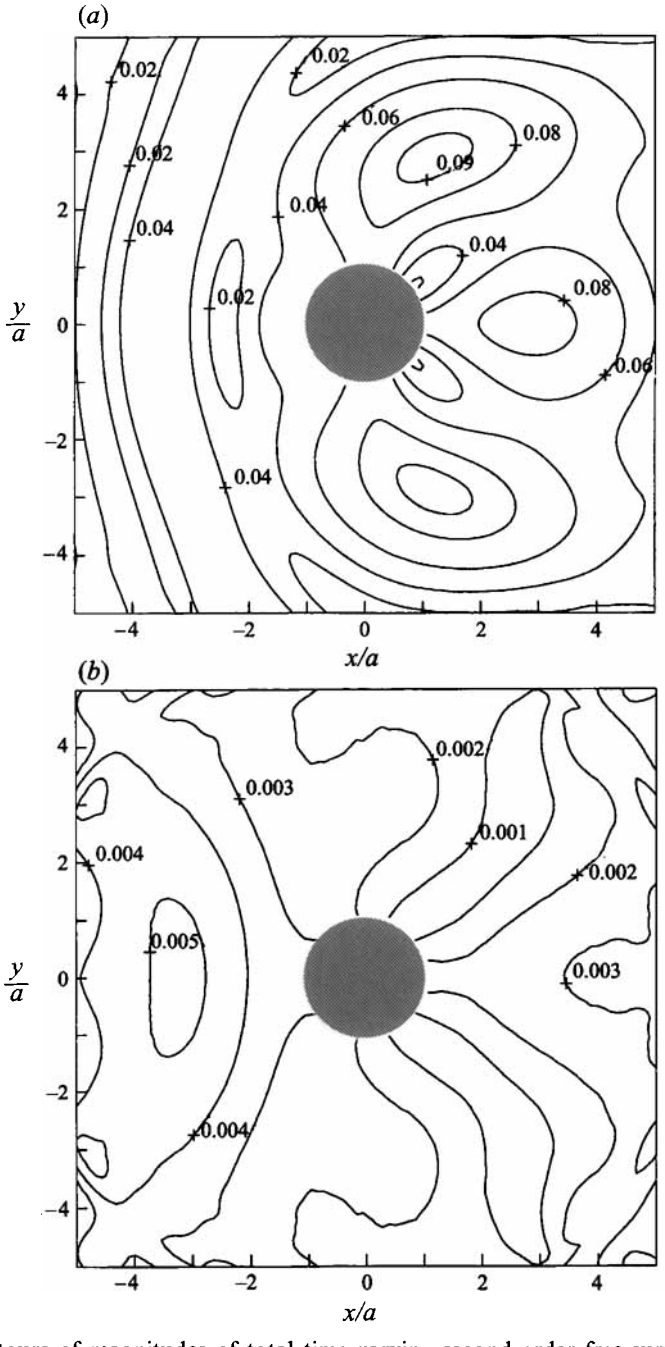

FIGURE 7. Contours of magnitudes of total time-varying second-order free-surface elevation (normalized by the wave amplitude A) for $ka = 0.4$, $kh = 8.0$. (a) Truncated cylinder with $b/a = 3.0$; (b) difference in amplitudes between a truncated cylinder and a bottom-seated cylinder in the same depth of water. Wave direction is from left to right.

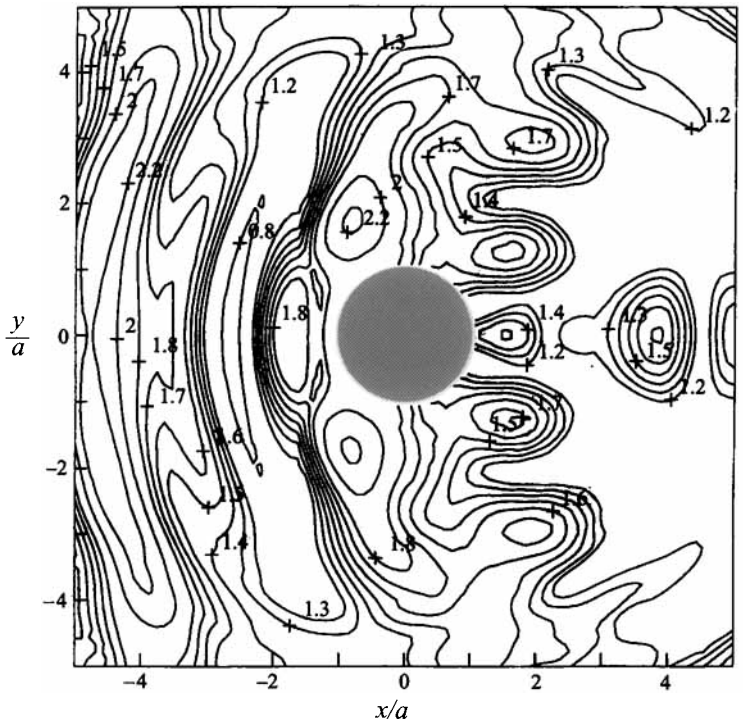

FIGURE 8. Contours of maximum total free-surface elevation (normalized by the wave amplitude A) for $ka = 0.4$, $kh = 8$, $b/a = 3.0$, $A/a = 0.3$. Wave direction is from left to right.

5.5. *Wave run-up on the body surface and the free-surface elevation*

We next investigate the wave elevation in the vicinity of the cylinder. Figure 5 shows the dimensionless amplitudes of first-order and components of second-order wave run-up along the waterline for two different incident wavenumbers. For comparison, results for a bottom-seated cylinder (with the same ka and kh) are also presented. Perhaps it is suprising that even for fairly small ka (e.g. $ka = 0.4$), the differences in both first-order and each component of second-order wave run-up between a truncated cylinder and a bottom-seated cylinder (with the same ka and kh) is negligibly small, indicating that the lower part of a bottom-seated cylinder does not make much contribution to the potentials at the waterline. The contour plots in figure 8 and figure 9 also show a similar phenomenon for the free-surface elevation near the cylinder. Figure 6(a) illustrates the amplitude of first-order free-surface elevation for a truncated cylinder ($b/a = 3$, $kb = 1.2$, $kh = 8$). Figure 6(b) shows the difference between the results for the truncated cylinder (figure 6a) and those for a bottom-seated cylinder in the same water depth. It is clear that the results for the two different geometries are remarkably close to each other. This implies that even with a moderate draught kb, the contribution of the lower part of a structure to the first-order potential on the free surface is relatively small. Figure 7 shows corresponding results for the amplitudes of the second-order free-surface elevation, again normalized by A and for $A/a = 0.1$. The contribution from the lower part of the bottom-seated cylinder is again seen to be small. These conclusions are very important in simplifying the second-order analysis of complex structures such as tension leg platforms.

Figure 8 shows the contours of maximum normalized free-surface elevation at the same frequency, but at a higher incident wave amplitude ($A/a = 0.3$). The surface

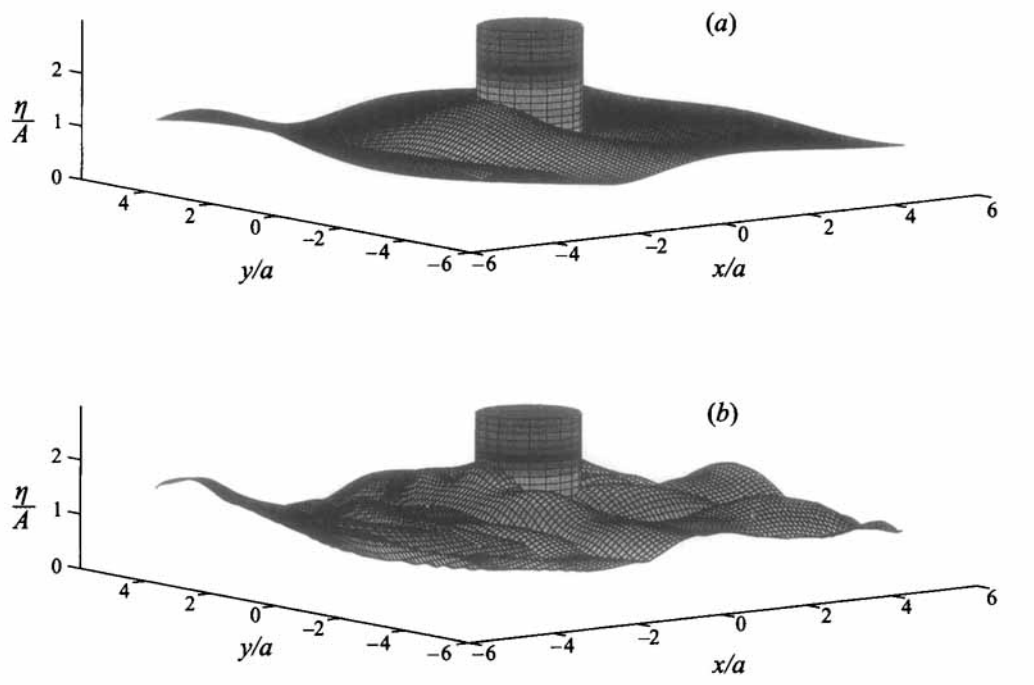

FIGURE 9. Isometrics of maximum free-surface elevation for $ka = 0.8$, $h/a = 4$, $A/a = 0.4$: (*a*) prediction by linear theory; (*b*) prediction by first- and second-order theory. Wave direction is from left to right.

contours have been evaluated as follows. At each spatial position, the sum of the linear component, the mean second-order component, and the component at twice the wave frequency, was calculated at 360 time steps during the wave period, and divided by the amplitude A of the incident wave. The maximum of the resulting 360 values was then used to define the surface at that position. The figure therefore provides an indication of the maximum elevation which would be observed in the vicinity of the cylinder; but it should be emphasized that the maxima at different positions occur at different times in the wave cycle. (If the same procedure were adopted for the linear component, the result would of course be identical to the contours of free-surface amplitude given in figure 6*a*.)

Similar results are shown as isometrics in figure 9, but now for a higher frequency corresponding to $ka = 0.8$. Figure 9(*a*) gives the predicted normalized elevation based on linear theory. The maximum normalized elevation shown in figure 9(*b*) includes both first- and second-order effects, for the case $A/a = 0.4$. The second-order contributions are seen to cause substantial local increases in the maximum wave elevation, for example in the vicinity of the upstream face of the truncated cylinder.

6. Conclusions

A complete semi-analytical solution has been given for second-order diffracted potential and associated quantities for a truncated circular cylinder in water of uniform finite depth. This solution provides an efficient and accurate (in the context of the second-order theory) means for analysing second-order wave loads as well as the free-surface elevation around a truncated vertical cylinder. Extension of this solution to a

third-order analysis would be straightforward, though much more complicated, and could provide a tool for estimating ringing loads. (Malenica & Molin 1994 have already considered the third-order problem for the bottom-seated circular cylinder, using a different approach). Another development would be to extend this solution to study second-order interaction between waves and multiple truncated cylinders, by adopting an appropriate interaction theory. This could lead to an efficient tool for second-order diffraction analysis of realistic offshore structures. Numerical results based on the present analysis show that in many cases the second-order loads on, and the free surface around, a truncated vertical cylinder are very close to those of a bottom-seated cylinder having the same radius in the same water depth, as long as in the latter case integration for the forces is carried out only on the upper part of the cylinder (i.e. the integrated height equals the draught of the truncated cylinder). This important conclusion suggests the route to development of an effective approximate solution for second-order potential and forces. By applying this idea to the multiple-cylinder interaction problems, such an approximate solution could dramatically reduce the computational effort in the second-order analysis for a structure such as a tension leg platform.

This work forms part of the research programme 'Uncertainties in Loads on Offshore Structures' sponsored by EPSRC through MTD Ltd and jointly funded with: Amoco (UK) Exploration Company, BP Exploration Operating Co. Ltd., Brown & Root, Exxon Production Research Company, Health and Safety Executive, Norwegian Contractors a.s., Shell UK Exploration and Production, Den Norske Stats Oljeselskap a.s., Texaco Britain Ltd.

Appendix A. Expressions for $[C_n^{(1)}]$, $[D_n^{(1)}]$, $\{E_n^{(1)}\}$

The terms of the matrices for the first-order analysis are as follows:

$$C_n^{(1)}(0,0) = \frac{n\sinh(kd)}{2(ka)(kh)[\gamma_0(m_0)]^{1/2}}, \tag{A 1}$$

$$C_n^{(1)}(j,0) = \frac{n\sin(m_j d)}{2(m_j a)(m_j h)[\gamma_j(m_j)]^{1/2}} \qquad (j = 1,2,\cdots), \tag{A 2}$$

$$C_n^{(1)}(0,m) = \frac{\lambda_m I_n'(\lambda_m a)}{I_n(\lambda_m a)} \frac{(-1)^m \sinh(kd)}{[k^2 + \lambda_m^2]h[\gamma_0(m_0)]^{1/2}}, \tag{A 3}$$

$$C_n^{(1)}(j,m) = \frac{\lambda_m I_n'(\lambda_m a)}{I_n(\lambda_m a)} \frac{(-1)^{m+1} \sin(m_j d)}{(\lambda_m{}^2 - m_j{}^2)h[\gamma_j(m_j)]^{1/2}}, \tag{A 4}$$

$$D_n^{(1)}(0,0) = \frac{2}{kd}\frac{H_n(ka)}{H_n'(ka)}\frac{\sinh(kd)}{[\gamma_0(m_0)]^{1/2}}, \quad D_n^{(1)}(j,0) = \frac{2k}{d}\frac{H_n(ka)}{H_n'(ka)}\frac{(-1)^j \sinh(kd)}{(\lambda_j^2 + k^2)[\gamma_0(m_0)]^{1/2}}, \tag{A 5, 6}$$

$$D_n^{(1)}(0,l) = \frac{2K_n(m_l a)}{K_n'(m_l a)} \frac{\sin(kd)}{m_l d[\gamma_l(m_l)]^{1/2}}, \tag{A7}$$

$$D_n^{(1)}(j,l) = \frac{2m_l}{d}\frac{K_n(m_l a)}{K_n'(m_l a)}\frac{(-1)^{l+1}\sin(m_l d)}{(\lambda_j^2 - m_l{}^2)][\gamma_j(m_j)]^{1/2}}, \tag{A8}$$

$$E_n^{(1)}(m) = \frac{2(-1)^m k P_n(ka)\sinh(kd)}{d(k^2 + \lambda_m{}^2)\cosh(kh)} \qquad (m = 0,1,2,\cdots). \tag{A9}$$

Appendix B. Expressions for $[C_n^{(2)}]$, $[D_n^{(2)}]$, $\{E_n^{(2)}\}$

The terms of the matrices for the second-order analysis can be shown to be

$$C_n^{(2)}(0,0) = \frac{n\sinh(k_0 d)}{2(k_0 a)(k_0 h)[\gamma_0(k_0)]^{1/2}}, \tag{B1}$$

$$C_n^{(2)}(m,0) = \frac{n\sin(k_m d)}{2(k_m a)(k_m h)[\gamma_m(k_m)]^{1/2}}, \qquad (m = 1,2,\cdots), \tag{B2}$$

$$C_n^{(2)}(0,l) = \frac{\lambda_l I_n'(\lambda_l a)}{I_n(\lambda_l a)} \frac{(-1)^l \sinh(k_0 d)}{[k_0^2 + \lambda_l^2]h[\gamma_0(k_0)]^{1/2}}, \tag{B3}$$

$$C_n^{(2)}(m,l) = \frac{\lambda_l I_n'(\lambda_l a)}{I_n(\lambda_l a)} \frac{(-1)^{l+1}\sin(k_m d)}{(\lambda_l{}^2 - k_m{}^2)h[\gamma_m(k_m)]^{1/2}}, \tag{B4}$$

$$D_n^{(2)}(0,0) = \frac{2}{k_0 d}\frac{H_n(k_0 a)}{H_n'(k_0 a)}\frac{\sinh(k_0 d)}{[\gamma_0(k_0)]^{1/2}}, \tag{B5}$$

$$D_n^{(2)}(m,0) = \frac{2k_0}{d}\frac{H_n(k_0 a)}{H_n'(k_0 a)}\frac{(-1)^m \sinh(k_0 d)}{(\lambda_m^2 + k_0^2)[\gamma_0(k_0)]^{1/2}}, \tag{B6}$$

$$D_n^{(2)}(0,l) = \frac{2K_n(k_l a)}{K_n'(k_l a)}\frac{\sin(k_l d)}{k_l d[\gamma_l(k_l)]^{1/2}}, \tag{B7}$$

$$D_n^{(2)}(m,l) = \frac{2k_l}{d}\frac{K_n(k_l a)}{K_n'(k_l a)}\frac{(-1)^{l+1}\sin(k_l d)}{(\lambda_m^2 - k_l{}^2)d][\gamma_l(k_l)]^{1/2}}. \tag{B8}$$

The functions γ_0 and γ_m are as defined in (2.15) and (2.16).

There is no convenient closed-form expression for $E_n^{(2)}(m)$. To evaluate these terms, we use a simple approximate quadrature. We divide the interval $[-h,-b]$ into N_j smaller intervals, assuming that in the jth interval, ($z \in [-\Delta z(j-1) - b, -j\Delta z - b]$, $\Delta z = d/N_j$), $\phi_{0n}^{(2)}(a,z)$ varies linearly with z. Therefore

$$\phi_{0n}(a,z) = \phi_{0n,j} + \frac{\phi_{0n,j+1} - \phi_{0n,j}}{\Delta z}(z_j - z). \tag{B9}$$

The equation for $E_n^{(2)}(m)$ then can be written as

$$E_n^{(2)}(m) = \frac{2}{h}\sum_{j=1}^{N_j}\int_{a_j}^{b_j}(\alpha_j + \beta_j z)\cos(\lambda_m(z+h))\mathrm{d}z, \tag{B10}$$

where

$$a_j = -(b + j\Delta z), \quad b_j = -b - (j-1)\Delta z,$$

$$\alpha_j = \phi_{0n,j} + \frac{\phi_{0n,j+1} - \phi_{0n,j+1}}{\Delta z} z_j, \quad \beta_j = \frac{\phi_{0n,j} - \phi_{0n,j+1}}{\Delta z}.$$

Hence we obtain

$$E_n^{(2)}(0) = \sum_{j=1}^{N_j}\left[\frac{\alpha_j(b_j - a_j)}{h} + \frac{1}{2h}\beta_j(b_j^2 - a_j^2)\right], \tag{B11}$$

$$E_n^{(2)}(m) = \sum_{j=1}^{N_j}\left\{\frac{2\alpha_j}{h\lambda_j}[\sin(\lambda_m(h+b_j)) - \sin(\lambda_m(h+a_j))] + \frac{2\beta_j}{\lambda_m h}\left[b_j\sin(\lambda_m(h+b_j))\right.\right.$$
$$\left.\left. - a_j\sin(\lambda_m(h+a_j)) + \frac{\cos(\lambda_m(b_j+h)) - \cos(\lambda_m(a_j+h))}{\lambda_m}\right]\right\}. \tag{B12}$$

Appendix C. Approximate expressions for quadratic components of the second-order forces on a truncated vertical cylinder

We give here expressions for quadratic components (mean and time-varying) of the second-order forces on a truncated vertical cylinder, due to the contribution of the approximated first-order potential. The surge force and pitch moment are considered, the latter being taken about an axis through the cylinder bottom. Since the quadratic component in heave is generally negligibly small, compared with the dynamic component due to the contribution of the second-order potential, it is not considered here.

The second-order mean surge force is

$$\frac{\overline{F}_x^{(2)}}{\rho g a A^2} = \frac{4}{\pi^2 (ka)^3}\left[\frac{\sinh(2kh)-\sinh(2kd)}{\sinh(2kh)} + \frac{2kb}{\sinh(2kh)}\right]\sum_{n=0}^{\infty}\frac{[1-n(n+1)/(ka)^2]^2}{|H_n'(ka)|^2|H_{n+1}'(ka)|^2}. \quad \text{(C1)}$$

The second-order mean pitch moment is

$$\frac{\overline{M}_y^{(2)}}{\rho g a A^2 b} = \mathrm{Re}\left\{\frac{-4i}{\pi(ka)^2}\sum_{n=0}^{\infty}\frac{1}{H_n'(ka)H_{n+1}'^{*}(ka)} \times\left[-1+\frac{2kb}{\sinh(2kh)}\left(\left(\frac{n(n+1)}{(ka)^2}+1\right)Z(kh)-\frac{1}{2}\right)\right]\right\}, \quad \text{(C2)}$$

where

$$Z(kh) = \frac{1}{4} + \frac{2kb\sinh(2kh)-\cosh(2kh)+\cosh(2kd)}{8k^2b^2}. \quad \text{(C3)}$$

The second-order time-varying quadratic surge force is

$$\frac{F_{xq}^{(2)}}{\rho g a A^2} = \frac{2i}{\pi(ka)^2}\sum_{n=0}^{\infty}\frac{(-1)^n}{H_n'(ka)H_{n+1}'(ka)}\left\{\left[2+\frac{\sinh(2kh)-\sinh(2kd)}{\sinh(2kh)} - \frac{2kb}{\sinh(2kh)}\right]+\frac{n(n+1)}{(ka)^2}\left[\frac{\sinh(2kh)-\sinh(2kd)}{\sinh(2kh)}+\frac{2kb}{\sinh(2kh)}\right]\right\}. \quad \text{(C4)}$$

The second-order time-varying quadratic pitch moment is

$$\frac{M_{yq}^{(2)}}{\rho g a A^2 b} = \frac{4i}{\pi(ka)^2}\sum_{n=0}^{\infty}\frac{(-1)^n}{H_n'(ka)H_{n+1}'(ka)}\left\{1+\frac{2kb}{\sinh(2kh)}\left[\left(1+\frac{n(n+1)}{(ka)^2}\right)Z(kh)-\frac{1}{2}\right]\right\}. \quad \text{(C5)}$$

REFERENCES

ABUL-AZM, A. G. & WILLIAMS, A. N. 1988 Second-order diffraction loads on truncated cylinders. *J. Waterway, Port, Coastal Ocean Div. ASCE* **114**, 436–454.

ABUL-AZM, A.G. & WILLIAMS, A. N. 1989*a* Approximation of second-order diffraction loads on arrays of vertical circular cylinders. *J. Fluids Struct.* **3**, 17–36.

ABUL-AZM, A.G. & WILLIAMS, A. N. 1989b Second-order diffraction loads on arrays of semi-immersed circular cylinder. *J. Fluids Struct.* **3**, 365–388.

CHAU, F. P. 1989 The second-order velocity potential for diffraction of waves by fixed offshore structures. PhD thesis, University College London, London University.

CHAU, F. P. & EATOCK TAYLOR, R. 1992 Second-order wave diffraction by a vertical cylinder. *J. Fluid Mech.* **240**, 571–599.

CHEN, X. & MOLIN, B. 1991 Calcul des efforts de deuxieme ordre a tres haute frequence sur des plates-forms a lignes tendues. *Proc. Troisieme Journees de l'Hydrodynamique*, pp. 133–146.

EATOCK TAYLOR, R. & CHAU, F. P. 1992 Wave diffraction theory, some developments in linear and nonlinear theory. *J. Offshore Mech. Arctic Engng* **114**, 185–194.

EATOCK TAYLOR, R. & HUANG, J. B. 1996 Application of second-order diffraction analysis to TLP design. *Final Report on Project A4, Managed Programme on Uncertainties in Loads on Offshore Structures*. University of Oxford.

EATOCK TAYLOR, R. & HUNG, S. M. 1987 Second-order diffraction forces on a vertical cylinder in regular waves. *Appl. Ocean Res.* **9**, 19–30.

GARRETT, C. J. R. 1971 Wave forces on a circular dock *J. Fluid Mech.* **46**, 129–139.

GHALAYINI, S. A. & WILLIAMS, A. N. 1991 Nonlinear wave forces on vertical cylinder arrays. *J. Fluids Struct.* **5**, 1–32.

KAGEMOTO, H. & YUE, D. K. P. 1986 Interaction among multiple three-dimensional bodies in water waves: an exact algebraic method. *J. Fluid Mech.* **166**, 189–209.

KIM, M. H. 1993 Second-harmonic vertical wave loads on arrays of deep draught circular cylinders in monchromatic uni- and multi-directional waves. *Appl. Ocean Res.* **15**, 245–262.

KIM, M. H. & YUE, D. K. P. 1989 The complete second-order diffraction solution for an axisymmetric body, Part 1, monochromatic waves. *J. Fluid Mech.* **200**, 235–264.

KIM, M. H. & YUE, D. K. P. 1990 The complete second-order diffraction solution for an axisymmetric body. Part 2. bichromatic incident waves and body motions. *J. Fluid Mech.* **211**, 557–593.

KRIEBEL, D. L. 1990 Nonlinear wave interaction with a vertical circular cylinder, part 1: diffraction theory. *Ocean Engng* **17**, 345–377.

KRIEBEL, D. L. 1992 Nonlinear wave interaction with a vertical circular cylinder, part 2: wave run-up. *Ocean Engng* **19**, 75–99.

LEE, C.-H., NEWMAN, J. N., KIM, M.-H. & YUE, D. K. P. 1991 The computation of second-order wave loads. *Proc. 10th Int. Conf. on Offshore Mechanics and Arctic Engineering*, I-A, pp. 113–123. ASME.

LEE, C.-H., & SCLAVOUNOS, P. D. 1989 Removing the irregular frequencies from integral equations in wave-body interactions. *J. Fluid Mech.* **207**, 393–418.

LIGHTHILL, M. J. 1979 Waves and hydrodynamic loading. *Proc. 2nd Intl. Conf. Behaviour Offshore Structures, BOSS London*, pp. 1–40.

LINTON, C. M. & EVANS, D. V. 1990 The interaction of waves with arrays of vertical circular cylinders. *J. Fluid Mech.* **215**, 549–569.

MALENICA, Š & MOLIN, B. 1994 Third order triple frequency wave forces on fixed vertical cylinders. *Proc. 9th Intl Workshop on Water Waves and Floating Bodies, Kyushu, Japan.*

MCIVER, P. & EVANS, D. V. 1984 Approximation of wave forces on cylinder arrays. *Appl. Ocean Res.* **6**, 101–107.

MOLIN, B. 1979 Second-order diffraction loads on three-dimensional bodies. *Appl. Ocean Res.* **1**, 197–212.

MOUBAYED, W. I. & WILLIAMS, A. N. 1994 The second-order diffraction loads and associated motions of a freely floating cylindrical body in regular waves: an eigenfunction expansion approach. *J. Fluids Struct.* **8**, 417–451.

MOUBAYED, W. I. & WILLIAMS, A. N. 1995 Second-order hydrodynamic interactions in an array of vertical cylinders in bichromatic waves. *J. Fluids Struct.* **9**, 61–98.

NEWMAN, J. N. 1990 Second harmonic wave diffraction at large depths. *J. Fluid Mech.* **213**, 59–70.

WILLIAMS, A. N., ABUL-AZM, A. G. & GHALAYINI, S. A. 1990 A comparison of complete and approximate solutions for second order diffraction loads on arrays of vertical cylinders. *Ocean Engng* **17**, 427–446.